Inverse Vernier effect in coupled lasers

Li Ge*
Department of Engineering Science and Physics, College of Staten Island, CUNY, Staten Island, New York 10314, USA and The Graduate Center, CUNY, New York, New York 10016, USA

Hakan E. Türeci
Department of Electrical Engineering, Princeton University, Princeton, New Jersey 08544, USA

(Received 22 April 2015; published 23 July 2015)

In this report we study the Vernier effect in coupled laser systems consisting of two cavities. We show that depending on the nature of their coupling, not only can the "supermodes" formed at overlapping resonances of these two cavities have the lowest thresholds as previously found, leading to lasing at these overlapping resonances and a manifestation of the typical Vernier effect, but also they can have increased thresholds and are hence suppressed, which can be viewed as an inverse Vernier effect. The inverse Vernier effect can also lead to an increased free spectrum range and possibly single-mode lasing, which may explain the experimental findings in several previous studies. We illustrate this effect using two coupled micro-ring cavities and a micro-ring cavity coupled to a slab cavity, and we discuss its relation to the existence of exceptional points in coupled lasers.

DOI: 10.1103/PhysRevA.92.013840 PACS number(s): 42.55.Sa, 42.55.Ah, 42.25.Hz

I. INTRODUCTION

The Vernier effect is well known in passive microwave and optical systems, which depict it as transmission resonances of a coupled system occurring when the resonances of the subsystems coincide. The counterpart of the Vernier effect in lasers has been experimentally studied with two or more coupled laser cavities, and an increased free spectral range (FSR) of the lasing spectrum and even single-mode lasing have been observed [1–8]. While some of these experiments utilized an interferometer [1–3] (type I; see Fig. 1) and can be understood similar to the Vernier effect in transmission, the others were different and consisted of fused or evanescently coupled slab and micro-ring or micro-disk cavities (type II). However, the understanding of the increased FSR or single-mode lasing in type II coupled systems is still often argued using the same mechanism as in type I systems, i.e., one cavity acts as an external cavity for frequency selection, and lasing occurs at the overlapping resonances of the individual laser cavities.

In this report we show that frequency overlap in type II systems does not favor lasing in general. Instead, the coupling of these overlapping resonances *increases* the lowest threshold of the corresponding lasing modes. Thus the increased FSR and single-mode lasing observed can be understood as a consequence of the suppression of these overlapping modes, which is the manifestation of an *inverse* Vernier effect. Below we illustrate this finding first in two evanescently coupled micro-ring cavities of different radii (see Fig. 1) and later in a micro-ring cavity coupled to a slab cavity. We show that the changes to the lasing thresholds are related to the existence of exceptional points (EPs) [9–18], at which two lasing modes have the same frequency, threshold, *and* spatial intensity pattern. We further show that the effect of coupling in type I systems increases with the detuning between two neighboring resonances, one in each of the two coupled cavities, while that in type II systems *decreases* with the detuning, yielding the inverse Vernier effect instead of the typical Vernier effect. Finally, we reveal that while the typical Vernier effect due to destructive interference does not impose any restrictions on the losses of the constituted cavities, the inverse Vernier effect depends on different losses, or equivalently different quality (Q) factors, in the two coupled cavities, highlighting its origin in coupling-caused Q spoiling.

Our analysis is based on the coupled-mode formulism suggested by Yariv [19], which takes into account the amplitude and phase evolutions inside the coupled cavities. Since the increased FSR and single-mode lasing reported in Refs. [4–8] were observed close to the lowest lasing threshold, nonlinearity was not crucial for these observations and we neglect it in the analysis below. We first consider two coupled micro-ring cavities (see Fig. 1), and the coupling between them can be captured by a scattering (S) matrix [19]:

$$\begin{pmatrix} a_{\rm out}^- \\ b_{\rm out}^+ \end{pmatrix} = S \begin{pmatrix} a_{\rm in}^- \\ b_{\rm in}^+ \end{pmatrix}, \quad S = \begin{pmatrix} t & J \\ -J^* & t^* \end{pmatrix}, \tag{1}$$

where $a_{\rm in,\,out}^-$ are the incoming and outgoing counterclockwise wave to the coupling junction in the first cavity, and $b_{\rm in,\,out}^+$ are similarly defined for the clockwise waves in the second cavity. The coupling of the waves traveling in the opposite directions, i.e., $a_{\rm in,\,out}^+$ and $b_{\rm in,\,out}^-$, is given by the same S matrix because of the local spatial symmetry at the coupling junction. We note that the S matrix is dimensionless, and so are t and J. They satisfy the local flux conservation relation $|t|^2 + |J|^2 = 1$, and the S matrix is unitary as a result. Since we do not expect a phase jump when $a_{\rm in}^-$ passes through the coupling junction to become part of $a_{\rm out}^-$, we take t to be real.

Assuming the circumferences of the two ring cavities are L_1 and L_2, the phase and amplitude changes of light after one circulation in each cavity and before coupling again is given by

$$a_{\rm in}^- = e^{i(n+i\kappa_1-i\tau)kL_1}\, a_{\rm out}^- \equiv \beta_1 a_{\rm out}^-, \tag{2}$$

$$b_{\rm in}^+ = e^{i(n+i\kappa_2-i\tau)kL_2}\, b_{\rm out}^+ \equiv \beta_2 b_{\rm out}^+, \tag{3}$$

*li.ge@csi.cuny.edu

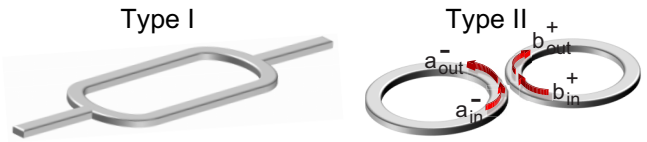

FIG. 1. (Color online) Schematics showing two types of coupled microcavities. Type I utilizes an explicit interferometer setup, while type II does not.

respectively. Here $k = \omega/c$ is the wave vector in free space and n is the refractive index of the ring cavities. The losses (radiation loss, material absorption, etc.) are represented by κ_1,κ_2 in these two cavities, respectively, and to focus on coupling-induced threshold changes we will treat them as constants for all modes. The optical gain is modeled by adding a negative imaginary part τ to n [20,21], and hence the laser threshold expressed in terms of τ is dimensionless.

By solving Eqs. (1) and (3), we find the following relation between the two counterclockwise amplitudes in the first micro-ring cavity

$$a_{\text{out}}^{-} = \frac{t-\beta_2}{1-t\beta_2}\, a_{\text{in}}^{-}, \tag{4}$$

from which the well-known critical coupling condition $t = \beta_2 \neq 1$ for a vanished a_{out}^{-} is readily seen. The lasing thresholds are determined by the self-consistent condition imposed by Eqs. (2) and (4), e.g., a_{in}^{-} should not change in steady-state lasing oscillation after light circulates the first ring cavity once and comes back to the same location:

$$\beta_1 \frac{t-\beta_2}{1-t\beta_2} = 1. \tag{5}$$

In the absence of coupling, i.e., $J = 0$ and $t = 1$, we recover the simple relation $\beta_1 = 1$ that determines the lasing frequencies and thresholds of the first micro-ring cavity, i.e.,

$$k_{1,m} = \frac{2\pi m}{nL_1}, \quad \tau_{1,m} = \kappa_1 \ (m = 1,2,\ldots).$$

Similarly, the lasing modes in the second micro-ring cavity are given by $k_{2,m} = 2\pi m/nL_2$ and $\tau_{2,m} = \kappa_2$. In order to recover the threshold condition of the second micro-ring cavity in the absence of coupling, i.e., $\beta_2 = 1$, it is necessary to rewrite Eq. (5) in the following equivalent form:

$$\beta_2 \frac{t-\beta_1}{1-t\beta_1} = 1. \tag{6}$$

In the strong coupling limit, i.e. $J \to 1$ and $t \to 0$, both Eqs. (5) and (6) become

$$\beta_1\beta_2 = -1, \tag{7}$$

which indicates that the system is now effectively a micro-ring cavity of circumference $(L_1 + L_2)$, with a π-phase shift (coming from the "$-$" sign) due to the coupling. We note that this result, as well as Eqs. (5) and (6), does not depend on the phase of the coupling J. As we show in Appendix A, the phase of J indeed bares no physical significance; it can be eliminated by shifting the phases of the propagating waves. Therefore, we take J to be real in the following discussions.

II. INVERSE VERNIER EFFECT

The FSRs of the uncoupled micro-ring cavities are $\Delta k_1 = 2\pi/nL_1$ and $\Delta k_2 = 2\pi/nL_2$, respectively. The average spectral density is then given by $\Delta k_1^{-1} + \Delta k_2^{-1}$, not counting the double degeneracy of the micro-ring resonances due to the clockwise and counterclockwise symmetry. Note that it is equal to the spectral density given by Eq. (7) at $J = 1$, where the lasing frequencies and thresholds are given by

$$k_m = \frac{(2m+1)\pi}{n(L_1+L_2)}, \tag{8}$$

$$\tau_m = \frac{L_1\kappa_1 + L_2\kappa_2}{L_1+L_2}. \tag{9}$$

This observation indicates that the lasing modes in the coupled system are evolved continuously from the uncoupled resonances as J increases from 0 to 1 [see Fig. 2(a)], with the ones originating from the larger ring cavity having the lower thresholds. The thresholds (9) at $J = 1$ are the same for all modes, given by the average of the thresholds of the uncoupled micro-ring cavities and weighted by the corresponding circumferences.

We note, however, this observation does not mean that the thresholds of the lasing modes have the same dependence on the coupling. As can be seen from Fig. 2(b) at $J = 0.5$, there is a clear difference between the thresholds of the lasing modes, which are inversely correlated with the detuning of the uncoupled resonances. The least overlapped resonances of the larger ring cavity have the lowest threshold and lase at a low pump power, while the better overlapped ones have higher thresholds and are suppressed at a low pump power. We refer to this effect as the *inverse* Vernier effect, since it is opposite to the Vernier effect in transmission that preserves

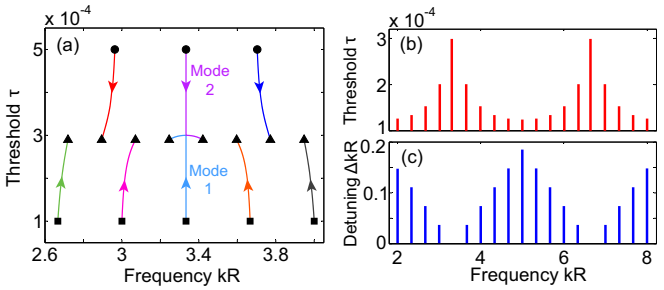

FIG. 2. (Color online) Inverse Vernier effect in two evanescently coupled micro-ring cavities. (a) Trajectories of the lasing thresholds versus the frequencies as the coupling J increases from 0 to 1. The squares and dots mark the uncoupled lasing modes at $J = 0$, respectively. The triangles show the coupled lasing modes at $J = 1$. Arrows indicate the direction of motion as J increases. R and $0.9R$ are the radius of the larger and smaller cavities, respectively. (b) Lowest thresholds of the lasing modes at $J = 0.5$, which are evolved from the uncoupled resonances in the larger ring cavity. Note the increased thresholds especially at the perfectly aligned resonances near $kR = 3.3,6.6$. (c) shows the detuning of these uncoupled resonances with the nearest counterparts in the smaller ring cavity. The total loss in the two cavities are $\kappa_1 = 10^{-4}$ and $\kappa_2 = 5 \times 10^{-4}$ respectively, corresponding to Q factors of 1.5×10^4 and 3×10^3. The refractive index is $n = 3$.

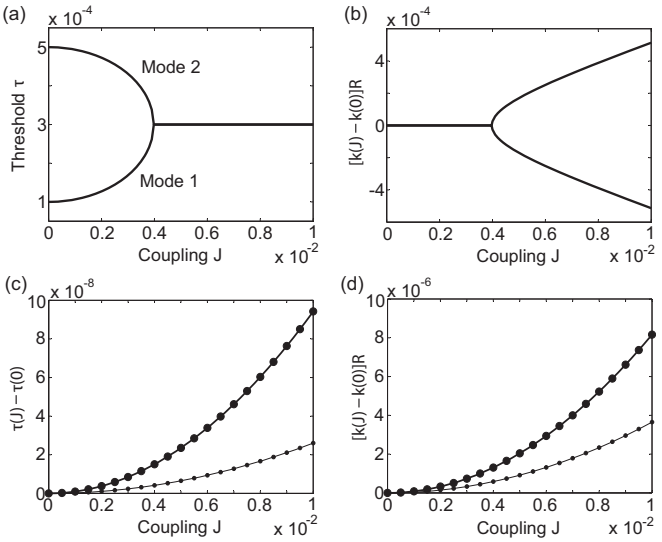

FIG. 3. Inverse bifurcation of the lasing frequencies (a) and bifurcation of the corresponding thresholds (b) of the perfectly aligned modes 1 and 2 near $kR = 3.3$ shown in Fig. 2(a), as the coupling increases from $J = 0$. The bifurcations occur near $J = 4 \times 10^{-3}$. The solid lines in (c) and (d) show the much weaker J dependencies of the two low-threshold modes on the left of mode 1 in Fig. 2(a), with the thin one farther away from mode 1. The dots show the analytical approximations given by Eqs. (16) and (17).

only the overlapping resonances. Nevertheless, the FSR of the active lasing modes can also be increased as a result and single-mode lasing may become possible if the gain spectrum is not too wide.

To better understand the much stronger J dependence of the thresholds at the spectrally aligned resonances [e.g., mode 1 of the larger cavity and mode 2 of the smaller cavity in Fig. 2(a)], we first note one of their qualitative differences from the detuned resonances. Starting from $J = 0$, modes 1 and 2 first move vertically in the k-τ plane when the coupling increases; they then coalesce before moving largely horizontally. The detuned resonances undergo avoided crossings instead. This behavior of modes 1 and 2 is plotted as a function of the coupling J in Figs. 3(a) and 3(b). Their frequencies and thresholds experience a bifurcation and inverse bifurcation respectively when J becomes $J_c \approx 4 \times 10^{-3}$, which indicate the existence of an EP [9–18]. In contrast, the detuned resonances show a much weaker J dependence when J is small, as shown in Figs. 3(c) and 3(d). At $J = J_c$ the threshold increase of mode 1 is more than 10^4 times larger than the detuned resonances.

The EPs are often studied in an eigenvalue problem [9–11]. Although in our coupled-mode formalism the threshold conditions (5) and (6) do not have the explicit form of an eigenvalue problem, the merging of the frequencies and thresholds of modes 1 and 2 shown in Figs. 2(a) and 3(a) and 3(b) at $J = J_c$ is a clear indication of an EP. This is further confirmed by the coalescence of their wave functions (see Fig. 4), which distinguishes an EP from a usual (Hermitian) degeneracy point. In the next section we will analyze the location of the EP as well as the much weaker J dependence of the detuned resonances.

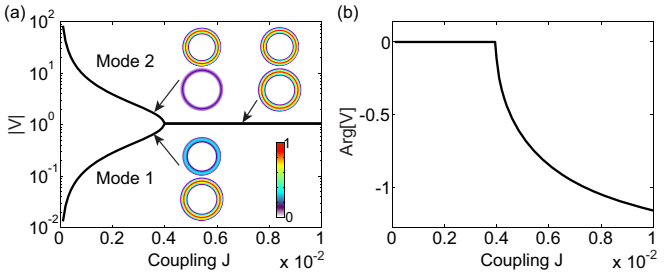

FIG. 4. (Color online) Ratio V of light amplitudes inside the two micro-ring cavities for modes 1 and 2 in Figs. 3(a) and 3(b). V is defined by Eqs. (10) and (11). The insets in (a) illustrate their different intensity ratios at $J = 3.5 \times 10^{-3}$ below the EP at $J_c = 4 \times 10^{-3}$ and their identical intensity ratio $|V| = 1$ at $J = 7 \times 10^{-3}$ above the EP. (b) The identical phase of V for modes 1 and 2, both below and beyond J_c.

III. ANALYTICAL RESULTS AND PHYSICAL INTERPRETATIONS

When the coupling is small, modes 1 and 2 concentrate in the larger and smaller micro-rings, respectively. This can be seen quantitatively from

$$V \equiv \frac{b_{\text{in}}^{+}}{a_{\text{in}}^{+}} = \frac{-\beta_2 J}{1 - t\beta_2} \tag{10}$$

for mode 1: the lasing condition of the first micro-ring cavity, i.e., $\beta_1 = 1$, holds for this mode when $J \to 0$, and $\beta_2 \neq 1$ because of the different thresholds of modes 1 and 2 when they are uncoupled. Therefore, $V \to 0$ for mode 1, which has little amplitude in the second micro-ring cavity as expected.

Similarly, V can be expressed as

$$V = \frac{1 - t\beta_1}{\beta_1 J} \tag{11}$$

for mode 2: the lasing condition of the second micro-ring cavity, i.e., $\beta_2 = 1$, holds for this mode when $J \to 0$, and $\beta_1 \neq 1$ because of the different thresholds of modes 1 and 2 when they are uncoupled. Therefore, $V \to \infty$ for mode 2, which has little amplitude in the first micro-ring cavity as expected.

We note that the two expressions (10) and (11) are mathematically identical using Eq. (5) or (6). We discussed them separately above just to avoid the ratio of two vanishing quantities in the limit $J \to 0$. Once J becomes finite, either expression can be used for both mode 1 and 2, and their V values (and hence their wave functions) become the same once they have the same value of β_1 (and consequently β_2 as well). This condition is satisfied when the frequencies and thresholds of these two modes become the same, i.e., at an EP.

To locate the EP in terms of the coupling J, we first note that $\beta_1 = \exp[(\tau - \kappa_1)k_0 L_1] \equiv \tilde{\beta}_1$ and $\beta_2 = \exp[(\tau - \kappa_2)k_0 L_2] \equiv \tilde{\beta}_2$ are both real at the aligned resonant frequency $k = k_0$. Consequently, Eq. (5) can be solved at $k = k_0$, with the threshold τ determined by

$$t = \frac{1 + \tilde{\beta}_1 \tilde{\beta}_2}{\tilde{\beta}_1 + \tilde{\beta}_2}. \tag{12}$$

For cavities of relatively high-quality factors (and hence with low loss), the exponents in $\tilde{\beta}_{1,2}$ are very small and we expand them to the second order of τ, which gives rise to

$$(\tau-\kappa_1)(\tau-\kappa_2)\approx\frac{2(t-1)}{k_0^2L_1L_2}. \tag{13}$$

The left-hand side depicts an quadratic curve of τ, with the minimum $(\kappa_1-\kappa_2)^2/4$ at $\tau=(\kappa_1+\kappa_2)/2$. If this minimum is lower than the constant on the right-hand side, i.e.,

$$t>1-\frac{k_0^2L_1L_2}{8}(\kappa_1-\kappa_2)^2, \tag{14}$$

or equivalently,

$$J<J_c\equiv\frac{1}{2}k_0\sqrt{L_1L_2}|\kappa_1-\kappa_2|, \tag{15}$$

Eq. (13) gives two real solutions of τ (i.e., modes 1 and 2). Right at $J=J_c$, these two solutions coalesce into one, and the EP is reached. If J is larger than J_c, then there is no solution to Eq. (12) with a real τ, which means that the corresponding modes can no longer exist at $k=k_0$, leading to the frequency bifurcation shown in Fig. 3(b).

Equation (15) gives $J_c=3.97\times10^{-3}$ for the example shown in Fig. 3, which agrees well with the numerical result shown. Equation (15) also shows that the toy model given in Ref. [17] is qualitatively correct, and the location of an EP in terms of the coupling is proportional to the difference of the losses in the two coupled cavities.

Similar to the derivation above, we obtain the approximations for the frequency and threshold changes of the lower-threshold modes, originating from the uncoupled resonances in the larger ring cavity:

$$\delta k(J)\equiv k(J)-k(0)\approx\frac{J^2}{2nL_1}\frac{\sin\theta}{1-\cos\theta}, \tag{16}$$

$$\delta\tau(J)\equiv\tau(J)-\tau(0)\approx\frac{(\kappa_2-\kappa_1)\delta k(J)}{\Delta}\frac{\theta}{\sin\theta}. \tag{17}$$

Here $\theta\equiv n\Delta L_2$ and Δ is the detuning of one resonant frequency in the larger ring from the nearest resonant frequency in the smaller ring. Equations (16) and (17) give excellent agreement with the numerical results when J is small, as can be seen from Figs. 3(c) and 3(d). They show that both δk and $\delta\tau$ are proportional to J^2 when J is small, and more importantly, these changes are inversely correlated with the detuning Δ when $|\theta|\ll1$, with $\delta k(J)$ proportional to Δ^{-1} and $\delta\tau(J)$ proportional to Δ^{-2} in this limit. Due to the two different FSRs of the two coupled cavities, the detuning Δ modulates as a function of frequency and so does the lasing threshold τ, which then leads to the inverse Vernier effect of the active lasing modes when the pump power is low.

This finding can be interpreted in the following way: for two cavities of different losses (and hence different Q factors), the coupling effect is strong for overlapping resonances, and the higher Q resonances are "spoiled" more by the lower Q ones, causing a significant increase of their thresholds. For little- or non-overlapping resonances, this Q-spoiling effect is weak, and hence the thresholds of the higher quality resonances do not vary much from their uncoupled values.

From this interpretation it is clear that different Q factors in the two coupled cavities are crucial for the inverse Vernier effect, which would not occur if the losses in the two micro-ring cavities are the same; this can be directly seen from Eq. (17), which shows that the lasing threshold τ does not change with the detuning Δ if $\kappa_1=\kappa_2$. A more rigorous proof without using the expansion for a small coupling J is given in Appendix B.

As we discussed above, the inverse Vernier effect in type II coupled systems is the result of detuning-dependent Q spoiling, due to the coupling to a lower Q cavity. The typical Vernier effect, on the other hand, is caused by the detuning-dependent destructive interference. To contrast their different dependencies on the detuning Δ, below we use the Michelson interferometer setup [1] to exemplify type I systems, the threshold condition of which is given by

$$\beta_1(k,\tau)T+\beta_2(k,\tau)R=1, \tag{18}$$

where $\beta_{1,2}=e^{i(n+i\kappa_{1,2}-i\tau)kL_{1,2}}$ are the phase and amplitude changes after one circulation along each arm of the Michelson interferometer. T and $R=1-T$ are the transmittance and reflectance of the beam splitter, and $L_{1,2},\kappa_{1,2}$ are the length and loss of each arm. For $T=0$ or 1, lasing in the two arms takes place independently.

For simplicity, we consider a 50/50 beam splitter ($T=R=0.5$), which simplifies the threshold condition to $\beta_1(k,\tau)+\beta_2(k,\tau)=2$. Similar to the derivation for the type II coupled systems, we find the threshold change of the higher Q modes is given by

$$\delta\tau=\tau(T=0.5)-\tau(T=0)\approx\frac{\cos\theta-1-\frac{L_2\sin^2\theta}{L_1+L_2\cos\theta}}{k_0L_1}. \tag{19}$$

We note that Eq. (19) is proportional to the detuning Δ^2 when $|\theta|\ll1$. In other words, the effect of coupling, or more precisely, the effect of destructive interference, is more pronounced for a larger detuning as expected. This is in stark contrast with the relation (17) for the threshold change in type II coupled systems ($\propto\Delta^{-2}$), which distinguishes the typical Vernier effect and the inverse Vernier effect reported here.

We also note that the difference of the losses, $\kappa_1-\kappa_2$, does not appear in Eq. (19); it is a higher order term for high-Q modes, or more specifically, when $|\kappa_1-\kappa_2|k_1L_2\ll1$. Thus the typical Vernier effect in type I systems is not related to Q spoiling due to the coupling to a lower Q cavity, while this mechanism is what causes the inverse Vernier effect in type II coupled systems as discussed.

IV. DISCUSSION AND CONCLUSION

Our analysis based on the coupled-mode formalism is general and can also be applied to, for example, a slab cavity coupled with a micro-ring or microdisk cavity. The only differences are (i) a different β factor is needed to capture the phase and amplitude change of the light after a round trip in the slab cavity, including the effect of the radiation loss through the end facets; and (ii) the clockwise and counterclockwise waves in the micro-ring or microdisk cavity are coupled by a slab resonance. More specifically, the equivalence of the threshold

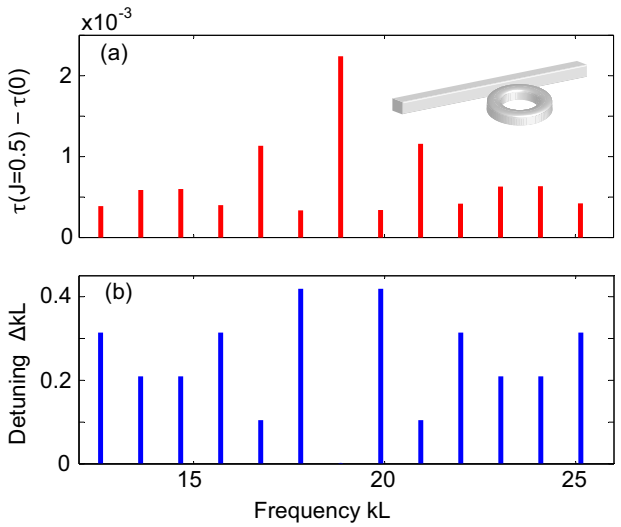

FIG. 5. (Color online) Inverse Vernier effect in a slab cavity of length L coupled with a micro-ring cavity of radius $R = L/1.8\pi$ [see the inset in (a)]. (a) Threshold changes for the lowest threshold modes near $kL = 20$ at $J = 0.5$. They originate from the uncoupled slab resonances, the loss of which is assumed to come from the radiation through two mirrors of reflectivity $r = 0.99$ and lower than that in the micro-ring ($\kappa = 5 \times 10^{-3}$). The threshold change is inversely correlated with the detuning from the nearest micro-ring resonance [see (b)].

condition (5) or (6) is

$$\beta_r \frac{t - \beta_s}{1 - t\beta_s} = 1, \tag{20}$$

where β_r is defined in the micro-ring cavity similar to β_1 in Eq. (2) and $\beta_s \equiv \pm e^{i(n+i\kappa_s - i\tau)kL}$ is defined in the slab cavity of length L and loss κ_s. If the radiation loss from the two mirrors of reflectivity r dominates in the slab, κ_s is then given approximately by $-\ln(r)/2kL$. The inverse Vernier effect still holds, as we show in Fig. 5.

In summary, we have shown that for two coupled cavities of different FSRs, the overlap of their resonances does not typically favor lasing except in an interferometer setup, resulting in an inverse Vernier effect. Nevertheless, the suppression of these overlapping resonances can also lead to an increased FSR and possibly single-mode lasing as well, as found in previous experiments [4–8]. We have treated J as a constant for all modes. If we consider a weaker value of the coupling due to a larger detuning, the differences of the maximum and minimum thresholds shown in Figs. 2(b) and 5(a) will be smaller, but their qualitative modulation as a function of the frequency still holds, and hence so does the inverse Vernier effect.

ACKNOWLEDGMENTS

We thank Peter Liu and Claire Gmachl for helpful discussions. L.G. acknowledges partial support by PSC-CUNY Cycle 46 Research Grant by the City University of New York and NSF Grant No. DMR-1506987. H.E.T. acknowledges NSF CAREER Grant No. DMR-1151810 and DARPA Grant No. N66001-11-1-4162.

APPENDIX A: PHASE OF THE COUPLING COEFFICIENT J

As we mentioned at the end of Sec. I, the phase of the coupling coefficient J does not appear in the threshold equations (5) and (6). Here we show explicitly that the phase of J can be eliminated by shifting the phases of the propagating waves $a^-_{\text{in, out}}$, $b^+_{\text{in, out}}$ in the coupled equation (1).

Suppose we start with a complex $J = J_0 e^{i\theta}$, where $J_0 = |J| > 0$. We then redefine

$$\tilde{a}^-_{\text{in, out}} \equiv a^-_{\text{in, out}} e^{-i\theta/2}, \quad \tilde{b}^+_{\text{in, out}} \equiv b^+_{\text{in, out}} e^{i\theta/2}, \tag{A1}$$

and introduce a transformation matrix O and its inverse O^{-1},

$$O = \begin{pmatrix} e^{-i\theta/2} & 0 \\ 0 & e^{i\theta/2} \end{pmatrix}, \quad O^{-1} \begin{pmatrix} e^{i\theta/2} & 0 \\ 0 & e^{-i\theta/2} \end{pmatrix}, \tag{A2}$$

satisfying $OO^{-1} = O^{-1}O = \mathbf{1}$, where $\mathbf{1}$ is the identity matrix. By multiplying O to both sides of Eq. (1), we find

$$\begin{aligned} \begin{pmatrix} \tilde{a}^-_{\text{out}} \\ \tilde{b}^+_{\text{out}} \end{pmatrix} &= O \begin{pmatrix} a^-_{\text{out}} \\ b^+_{\text{out}} \end{pmatrix} = O \begin{pmatrix} t & J \\ -J^* & t^* \end{pmatrix} \begin{pmatrix} a^-_{\text{in}} \\ b^+_{\text{in}} \end{pmatrix} \\ &= O \begin{pmatrix} t & J \\ -J^* & t^* \end{pmatrix} O^{-1} O \begin{pmatrix} a^-_{\text{in}} \\ b^+_{\text{in}} \end{pmatrix} \\ &= O \begin{pmatrix} t & J \\ -J^* & t^* \end{pmatrix} O^{-1} \begin{pmatrix} \tilde{a}^-_{\text{in}} \\ \tilde{b}^+_{\text{in}} \end{pmatrix}. \end{aligned} \tag{A3}$$

In other words, the S matrix for the phase-shifted waves $\tilde{a}^-_{\text{in, out}}, \tilde{b}^+_{\text{in, out}}$ are

$$\begin{aligned} \tilde{S} &= O \begin{pmatrix} t & J \\ -J^* & t^* \end{pmatrix} O^{-1} \\ &= \begin{pmatrix} e^{-i\theta/2} & 0 \\ 0 & e^{i\theta/2} \end{pmatrix} \begin{pmatrix} t & J_0 e^{i\theta} \\ -J_0 e^{-i\theta} & t^* \end{pmatrix} \begin{pmatrix} e^{i\theta/2} & 0 \\ 0 & e^{-i\theta/2} \end{pmatrix} \\ &= \begin{pmatrix} t & J_0 \\ -J_0 & t^* \end{pmatrix}, \end{aligned} \tag{A4}$$

in which the coupling is now real.

APPENDIX B: ROLE OF DIFFERENT CAVITY LOSSES

In the main text we discussed that the different losses in coupled cavities is the key factor that leads to the inverse

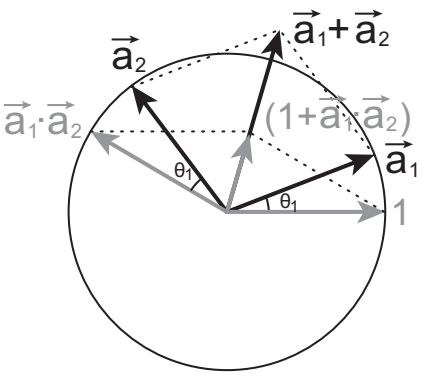

FIG. 6. Schematics showing the right-hand side of Eq. (B1).

Vernier effect. It was presented using physical intuitions and the expansion of the threshold condition in the weak coupling limit ($J \ll 1$). Here we show more rigorously that the lasing threshold τ does not change with the coupling J if the coupled cavities have the same loss, i.e., $\kappa_1 = \kappa_2$, and hence the inverse Vernier effect does not occur in this case.

What we do is the following: we take τ to be equal to $\kappa_1 = \kappa_2$, and show that the resulting threshold condition

$$t \in [0,1] = \frac{1 + e^{ink(\theta_1+\theta_2)}}{e^{i\theta_1} + e^{i\theta_2}} \tag{B1}$$

can be satisfied simply by varying the lasing frequency k. Here $\theta_1 \equiv nkL_1$ and $\theta_2 \equiv nkL_2$ are the phase changes in the two ring cavities after a round trip. We note that the right-hand side of Eq. (B1) depicts the sum of two unit vectors $\vec{a}_1$,$\vec{a}_2$ dividing the sum of their inner product $(\vec{a}_1 \cdot \vec{a}_2)$ and the unit vector along the real axis. From the phasor diagram shown in Fig. 6, we know that these two sums are both along the bisector of the angle formed by $\vec{a}_1$ and $\vec{a}_2$, because $\vec{a}_1 \cdot \vec{a}_2$ is rotated counterclockwise from $\vec{a}_2$ by the same angle θ_1 between 1 and $\vec{a}_1$. Therefore, their ratio is indeed real as required by Eq. (B1). Equation (B1) at any coupling $J = \sqrt{1 - t^2}$ can then be satisfied by varying θ_1 and θ_2 via k, which changes the ratio of the two aforementioned sums.

[1] M. DiDomenico, IEEE J. Quantum Electron. **QE-2**, 311 (1966).
[2] P. Q. Liu, X. Wang, and C. F. Gmachl, Appl. Phys. Lett. **101**, 161115 (2012).
[3] M. C. Zheng, P. Q. Liu, X. Wang, J.-Y. Fan, M. Troccoli, and C. F. Gmachl, Appl. Phys. Lett. **103**, 211112 (2013).
[4] P. Q. Liu, X. Wang, J.-Y. Fan, and C. F. Gmachl, Appl. Phys. Lett. **98**, 061110 (2011).
[5] P. Q. Liu, K. Sladek, X. Wang, J.-Y. Fan, and C. F. Gmachl, Appl. Phys. Lett. **99**, 241112 (2011).
[6] L. Shang, L. Liu, and L. Xu, Opt. Lett. **33**, 1150 (2008).
[7] X. Wu, H. Li, L. Liu, and L. Xu, Appl. Phys. Lett. **93**, 081105 (2008).
[8] E. Mujagić, C. Schwarzer, W. Schrenk, Y. Yao, J. Chen, C. Gmach, and G. Strasser, Opt. Eng. **49**, 111113 (2010).
[9] J. Okołowicz, M. Płoszajczak, and I. Rotter, Phys. Rep. **374**, 271 (2003).
[10] W. D. Heiss, J. Phys. A: Math. Gen. **37**, 2455 (2004).
[11] M. V. Berry, Czechoslovak J. Phys. **54**, 1039 (2004).
[12] N. Moiseyev, *Non-Hermitian Quantum Mechanics* (Cambridge University, New York, 2011).
[13] C. Dembowski, H.-D. Gräf, H. L. Harney, A. Heine, W. D. Heiss, H. Rehfeld, and A. Richter, Phys. Rev. Lett. **86**, 787 (2001).
[14] J. Wiersig, S.-W. Kim, and M. Hentschel, Phys. Rev. A **78**, 053809 (2008).
[15] S.-B. Lee, J. Yang, S. Moon, S.-Y. Lee, J.-Bo Shim, S. W. Kim, J.-H. Lee, and K. An, Phys. Rev. Lett. **103**, 134101 (2009).
[16] M. Liertzer, L. Ge, A. Cerjan, A. D. Stone, H. E. Türeci, and S. Rotter, Phys. Rev. Lett. **108**, 173901 (2012).
[17] R. El-Ganainy, M. Khajavikhan, and L. Ge, Phys. Rev. A **90**, 013802 (2014).
[18] C. M. Gentry and M. A. Popović, Opt. Lett. **39**, 4136 (2014).
[19] A. Yariv, Electron. Lett. **36**, 321 (2000).
[20] L. Ge, Y. D. Chong, S. Rotter, H. E. Türeci, and A. D. Stone, Phys. Rev. A **84**, 023820 (2011).
[21] J. Andreasen, C. Vanneste, L. Ge, and H. Cao, Phys. Rev. A **81**, 043818 (2010).